Communication

Competitive Multiple-Mechanism-Driven Electrochemiluminescent Detection of 8-Hydroxy-2'-deoxyguanosine

Yanqin Lv, Shiyu Chen, Yanfei Shen, Jingjing Ji, Qing Zhou, Songqin Liu, and Yuanjian Zhang

J. Am. Chem. Soc., **Just Accepted Manuscript** • DOI: 10.1021/jacs.8b00515 • Publication Date (Web): 14 Feb 2018

Competitive Multiple-Mechanism-Driven Electrochemiluminescent Detection of 8-Hydroxy-2′-deoxyguanosine

Yanqin Lv, Shiyu Chen, Yanfei Shen, Jingjing Ji, Qing Zhou, Songqin Liu, Yuanjian Zhang*

Jiangsu Engineering Laboratory of Smart Carbon-Rich Materials and Device, Jiangsu Province Hi-Tech Key Laboratory for Bio-Medical Research, School of Chemistry and Chemical Engineering, Medical School, Southeast University, Nanjing 211189, China, Email: Yuanjian.Zhang@seu.edu.cn

Supporting Information Placeholder

ABSTRACT: Natural selection over billions of years has developed highly effective in vivo signal transduction that is often governed by a series of competitive multiple mechanisms. Several artificial signal transduction pathways have inspired numerous biosensing systems, however, most of these are driven by a single mechanism. Herein, we describe a multiple-mechanism-driven electrochemiluminescent (ECL) biosensor that utilizes competitive catalytic and steric hindrance effects by assembling hemin/G-quadruplex on the carbon nitride nanosheets. Taking detecting 8-Hydroxy-2'-deoxyguanosine (8-OHdG) as example, the integrated dynamic ranges of the detectable concentration from each mechanism were achieved in a single sensor interface. Moreover, the detection sensitivity was more precisely controlled by the competition between the two mechanisms, and inherently boosted, compared to that of the single mechanism-driven detection. Going beyond the conventional single mechanism-driven biosensing, the elaborately biomimetic coupling of multiple mechanisms in a single interface may open a new approach for future multiplexed biosensing.

Exploring biosensors for sensitive detection of important biomarkers is of ongoing interest for early disease diagnosis, treatment and management.[1] Generally, the biosensing system consists of two primary elements responsible for the biomolecules recognition and signal reporting, respectively.[2] Hence, great efforts have been devoted to not only obtaining highly selective recognition but also to the development of new signal transduction pathways to enable quantitative analysis. Among these, several signal transduction pathways that rely on the catalytic reactions,[3] steric hindrance effect,[4] resonance energy transfer,[5] and charge transfer[6] have inspired numerous biosensing studies. For instance, except for conventional high-performance liquid chromatography,[7] 8-hydroxy-2'-deoxyguanosine (8–OHdG), an important biomarker for DNA oxidative damage,[8] was recently detected by charge transfer or steric hindrance effect-based signal transduction via spectroscopic[9] and electrochemical methods[10]. This leads to a more comprehensive understanding of each sensing mechanism that has its own characteristic set of advantages and limitations. However, most previous biosensors are driven by a single sensing mechanism,[3a, 4-6] and the sensing system regulated by competitive multiple mechanisms was rarely reported.[5e]

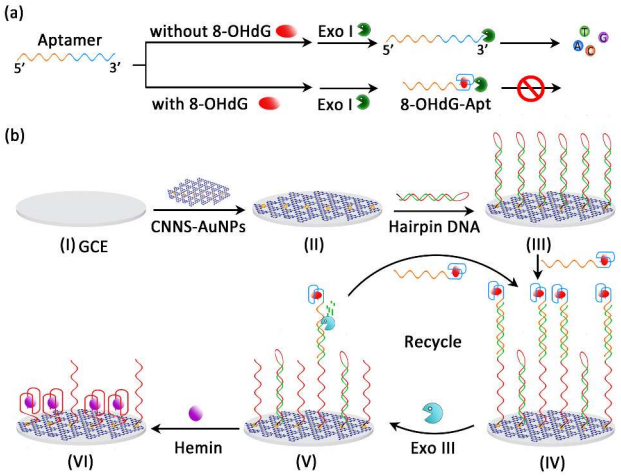

Figure 1. Assembly procedures of dual mechanism-driven ECL biosensor for 8–OHdG.

Natural selection over billions of years has already developed highly effective in vivo signal transduction, which is often governed by a series of competitive multiple mechanisms. For example, the catalytic metabolism of glucose was modulated not only allosterically by adenosine monophosphate, an activator of phosphorylase b, but also by several other inhibitor molecules.[11] By biomimicking the ingenuity of nature, the development of multiple-mechanism driven signal transduction system would provide a new approach to further boost the biosensing performance. Herein, we report the integration of a competitive catalytic reaction and steric hindrance effect into a single electrochemiluminescent (ECL) biosensor interface by assembling hemin/G-quadruplex on carbon nitride nanosheets. As an example, 8–OHdG, was detected by the dual-mechanisms driven biosensor with a much higher sensitivity and boarder calibration curves range compared to by previous methods.

Figure 1 shows the processes for fabricating a dual mechanism-driven ECL biosensor for 8–OHdG. The carbon nitride nanosheets (CNNS) obtained by liquid exfoliation of bulk polymeric carbon nitride were selected as the luminophor [12] due to their adjustable nanostructures, surface and luminescent properties and other advantages.[13] To further improve

the conductivity of CNNS and enhance the bioconjugation reliability of the hairpin probe, homogeneous Au nanoparticles (AuNPs, ca. 5 nm, 20.4 wt %) were facilely deposited on the CNNS (Fig. S1-S3). Based on the profiles of the ECL spectra (Fig. S1c) and ECL stability (Fig. S4), the loading of AuNPs did not alter the original ECL of CNNS.

To introduce two competitive mechanisms in the single ECL biosensor, a hemin/G-quadruplex assembly was conjugated to CNNS-AuNPs on glassy carbon electrode (GCE). Briefly, a –SH group terminated hairpin probe containing a recognition sequence for the aptamer probe (green part) and a "caged" G-quadruplex sequence (red part), was covalently attached to CNNS-AuNPs via Au-S bond (Fig. 1). The aptamer probe was protected after the targeted 8–OHdG was captured. Two kinds of exonuclease (Exo I & III) were then introduced to digest the unbound aptamer probes and release the protected aptamer probes (8-OHdG-Apt), respectively.[14] Recycling of 8-OHdG-Apt led to the continuous opening of the hairpin probe and the generation of "active" G-quadruplex structures. Finally, by adding hemin, the liberated G-quadruplexes were folded into a supramolecular hemin/G-quadruplex (see Fig S5 and more discussion in SI).[15] Each successful assembly step on GCE was verified by electrochemical impedance spectroscopy (EIS, Fig. S1d).[16]

The hemin/G-quadruplex assembly was designed to be dual-functional. On the one hand, the ECL of CNNS-AuNPs was quenchable by H_2O_2 (Fig. S6), while as a horseradish peroxidase-mimicking DNAzyme, the hemin/G-quadruplex could convert H_2O_2 into OH^- by two catalytic steps (Eq. S1-2).[17] Hence, the inhibition for ECL of CNNS-AuNPs by such H_2O_2 would be relieved if the catalytic conversion of H_2O_2 occurred. To support this hypothesis, a low concentration of 8–OHdG (10^{-16} M) was introduced into the biosensing system. As shown in Fig. 2a, the cathode reduction current was much higher than that without 8-OHdG, suggesting the occurrence of an electrocatalytic reduction process of H_2O_2 due to the formation of hemin/G-quadruplex. Accordingly, an improved ECL intensity of CNNS-AuNPs was observed.

On the other hand, because hemin/G-quadruplex has a much higher space charge density than hairpin probe-DNA,[18] the assembly of hemin/G-quadruplex on CNNS-AuNPs, especially for a large amount, would in turn limit the electron transfer and the free mass diffusion of $S_2O_8^{2-}$ co-reagent to approach the vicinity of CNNS. When such steric hindrances were dominant, the ECL of CNNS would be suppressed. To verify this assumption, EIS was used to investigate the modified GCE after the addition of 8–OHdG with different concentrations. As shown in Figure 2c, the charge-transfer resistance (R_{ct}) slightly increased from 2018 to 2672 Ω when the concentration of 8–OHdG is low, e.g., ranging from 0 to 10^{-16} M. However, the R_{ct} increased remarkably from 3664 to 7685 Ω when the concentration of 8–OHdG became higher, e.g., rising from 10^{-14} to 10^{-6} M (Fig. 2d). Accordingly, in the latter case, a significant decrease of the ECL intensity of CNNS-AuNPs was observed (Fig. 2b).

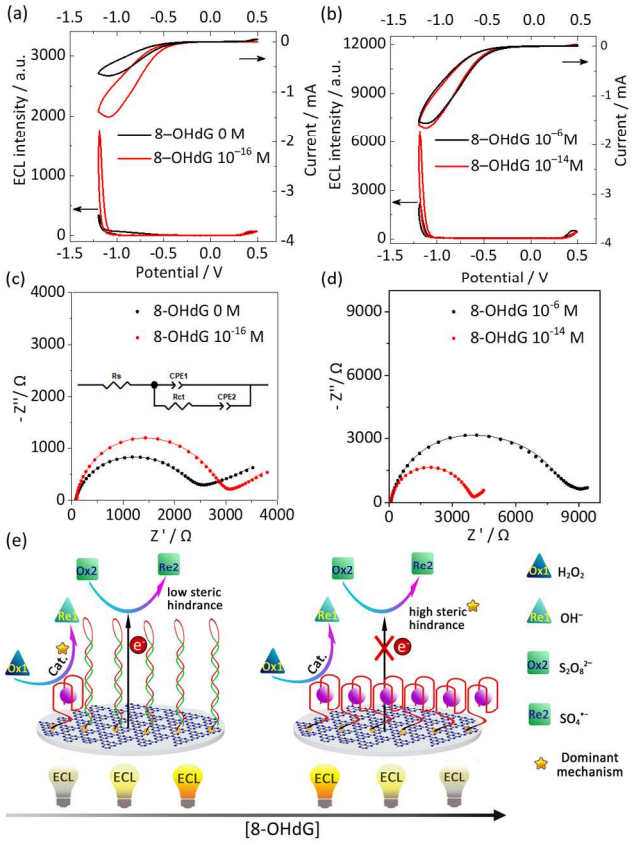

Figure 2. (a) ECL responses and (b) cyclic voltammetry curves of H_2O_2 reduction (10 mM) and (c, d) Nyquist plots (scatters) and simulation (lines) of the dual mechanism-driven biosensor without and with a low concentration (a and c, 10^{-16} M) and high concentration of (b and d, 10^{-14} and 10^{-6} M) targeted 8–OHdG. Inset in (c) shows the equivalent circuit. (e) Proposed reactions occurred at the dual mechanism-driven biosensor with low (left) and high (high) concentration of 8–OHdG.

These results suggested that the hemin/G-quadruplex assembly was dual-functional for the ECL of CNNS-AuNPs. Upon the capture of the targeted 8–OHdG, although the as-generated hemin/G-quadruplex would remove the inhibition of H_2O_2 for ECL of CNNS-AuNPs by catalytic reactions,[17] the steric hindrance effect from hemin/G-quadruplex itself conversely led to the decrease of the ECL intensity of CNNS-AuNPs. Interestingly, such two contradictory mechanisms could be modulated by different concentrations of 8–OHdG. At low concentration of 8–OHdG, only very few hemin/G-quadruplex was formed and the R_{ct} was negligible (Fig. 2e, left). Therefore, the electrocatalytic reduction of H_2O_2 by the hemin/G-quadruplex, i.e., the ECL recovering process, mostly determined the ECL intensity of CNNS-AuNPs. By contrast, at high concentration of 8–OHdG, a substantial amount of hemin/G-quadruplex was formed, the R_{ct} of which could not be ignored (Fig. 2e, right),[19] making the steric hindrance dominate the ECL intensity of CNNS-AuNPs.

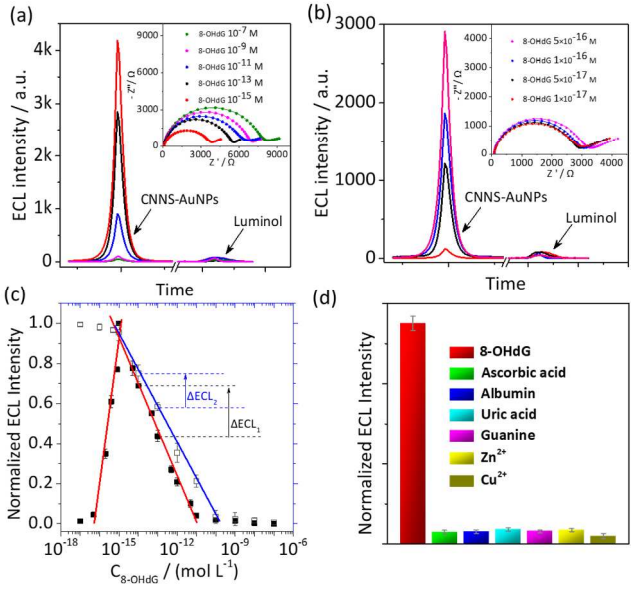

Figure 3. ECL profiles of the competitive dual mechanisms-driven ECL biosensor for 8–OHdG with high concentrations ranging from 10^{-7} to 10^{-15} M (a) and with low concentrations ranging from 10^{-17} to 5×10^{-16} M (b). Insets show the corresponding Nyquist plots (scatters) and simulation (lines). (c) Calibration curves for 8–OHdG detection by the dual mechanisms-driven ECL biosensor (■) and the single steric hindrance effect-driven ECL biosensor (□). (d) Selectivity of the dual mechanisms-driven ECL biosensor.

To apply the competitive dual-mechanism for realistic biosensing of 8–OHdG, a build-in correction for a variety of analyte-independent factors was further adopted by adding luminol into the electrolytes as an internal anodic reference luminophor (Fig. S7).[20] After the optimization of the sensing conditions such as the cleavage time for Exo III, and the concentrations of the co-reagents and internal luminol (Fig. S8), the dynamic range for detecting 8–OHdG was first examined. When the concentration of 8–OHdG decreased from the pM level, the ECL intensity of CNNS-AuNPs increased (Fig. 3a) gradually along with the evident impedance decrease (Fig. 3a inset, R_{ct} decreased from 7306 to 3320 Ω). The logarithmic value of the ECL intensity showed a linear dependence on the 8–OHdG concentration ranging from 10^{-15}~10^{-12} M with the correlation coefficient of 0.998. As a control, the ECL biosensor only using the steric hindrance effect was prepared (see details in SI). Strikingly, the slope of the calibration curves of the dual mechanism-driven ECL biosensor was higher than that of the steric hindrance effect-driven one. It was supposed that the catalytic reduction of H_2O_2 in the dual mechanism-driven ECL biosensor may still be in favor of ECL recovery at high concentration of 8–OHdG, but this effect was negligible with respect to the steric hindrance effect that dominated the evident decrease. Moreover, the catalytic reduction of H_2O_2 would also consume the limited electrons from GCE, further suppressing the ECL reactions (Eq. 3-9). Therefore, the dual mechanism-driven ECL biosensor showed higher ECL signal changes ($\Delta ECL_1 > \Delta ECL_2$) upon the same variation of the 8–OHdG concentration, i.e., a superior sensitivity, which inherently originated from the competition between the catalytic/steric hindrance effects.

Interestingly, when the concentration of 8–OHdG further decreased to 10^{-17} M, the ECL intensity of CNNS-AuNPs in the competitive dual mechanism-driven ECL biosensor decreased gradually with the decrease of the 8–OHdG concentration (Fig. 3b); notably, during this process, almost no significant impedance changes were observed (Fig. 3b inset, R_{ct} slightly increased from 2468 to 2871 Ω). The logarithmic value of the normalized ECL intensity showed a linear scaling with the concentration of 8–OHdG from 1 fM to 50 aM with the correlation coefficient of 0.991 (Fig. 3c), indicating that the detectable concentration for 8-OHdG could be further downshifted by two orders of magnitude. The detection limit was calculated to be 38.8 aM (S/N=3), much lower than that for the best previously reported biosensors (Table S1). By contrast, for the single steric hindrance effects-driven ECL biosensor, the ECL signal almost reached a plateau and could not show any useful dependence on such ultra-low concentration (Fig. 3c).

To investigate the feasibility of this approach in complex biological matrices, we applied this assay for the detection of 8–OHdG in human serum that contains a variety of proteins and other potential interferences. Standardized human serum samples were spiked with 8–OHdG of different concentrations. Since the calibration curves were bell-shaped, in order to reliably determine the concentration of 8–OHdG, each 8–OHdG sample in serum was measured after being diluted 5- and 10-fold, respectively. If the ECL intensity of the diluted sample increased, the calibration curve with the negative slope was used to calculate the concentration. Otherwise, another calibration curve with a positive slope was used. The results by averaging three independent determinations are summarized in Table S2. The recoveries ranged from 90% to 108% and the relative standard derivations were in the range of 3.5% to 5.1%, indicating that the proposed competitive dual-mechanism driven biosensing had good accuracy and high precision (see more discussion in in SI). Admittedly, our sensing strategy provided two linear ranges, leading to at least two measurements for the reliable determination of the 8–OHdG concentration. Nevertheless, by coupling two competitive mechanisms, not only the integrated dynamic ranges of detectable concentration from each mechanism were achieved in a single sensor interface which would undoubtedly simplify the biosensor fabrication and operation but also the sensitivity was inherently boosted with respect to that of a single mechanism-driven sensor. The binding specificity of the proposed biosensor was also studied. Various 8–OHdG interferents of the same concentration (10^{-14} M)[8] were individually added into the biosensing system, but this only exhibited a negligible change of ECL (Figure 3d). This indicated that the aptameric recognition function in the competitive dual mechanism-driven biosensor system was retained well and had sufficient selectivity for 8–OHdG.

In summary, we have developed a biomimetic ECL biosensor for 8–OHdG based on two competitive catalytic/steric hindrance mechanisms by assembling hemin/G-quadruplex on CNNS. The integrated dynamic ranges of the detectable concentration from each mechanism could be obtained in a single sensor interface, which was supposed to simplify the current biosensor fabrication and operation. Moreover, due to the delicate competition between the two mechanisms, the detecting sensitivity was also inherently boosted, com-

pared to that of single mechanism-driven sensors. These superior sensing performances were inherently originated from the unique biosensing interface driven by competitive multiple mechanisms. For practical applications, the proposed multiple-mechanism driven biosensor still requires many optimizations for greater simplicity and lower cost, and for instrumentation use in future works. Biomimicking the ingenuity of nature to change from a conventional single-mechanism driven biosensor to a multiple mechanism driven one would provide a new approach to further boost the performances of biosensors.

ASSOCIATED CONTENT

Supporting Information

Experimental, TEM, ECL/EIS/XRD/UV-vis absorption spectra, CV curves, table and more control results and supplementary discussion. This material is available free of charge via the Internet at http://pubs.acs.org

AUTHOR INFORMATION

Corresponding Author

Yuanjian.Zhang@seu.edu.cn

ACKNOWLEDGMENT

This work was supported by the National Natural Science Foundation of China (21775018, 21675022), the Natural Science Foundation of Jiangsu Province (BK20160028, BK20170084), the Open Funds of the State Key Laboratory of Electroanalytical Chemistry (SKLEAC201703) and the Fundamental Research Funds for the Central Universities.

REFERENCES

(1) Chinen, A. B.; Guan, C. M.; Ferrer, J. R.; Barnaby, S. N.; Merkel, T. J.; Mirkin, C. A., *Chem. Rev.***2015,** *115*, 10530.

(2) Chen, Y.; Zhou, S.; Li, L.; Zhu, J. j., *Nano Today.***2017,** *12*, 98.

(3) a) Lu, J.; Do, I.; Drzal, L. T.; Worden, R. M.; Lee, I., *ACS Nano.***2008,** *2*, 1825; b) Wu, Z.; Fan, H.; Satyavolu, N. S. R.; Wang, W.; Lake, R.; Jiang, J.-H.; Lu, Y., *Angew. Chem. Int. Ed.***2017,** *56*, 8721.

(4) a) de-los-Santos-Álvarez, N.; Lobo-Castañón, M. J.; Miranda-Ordieres, A. J.; Tuñón-Blanco, P., *J. Am. Chem. Soc.***2007,** *129*, 3808; b) Mahshid, S. S.; Camiré, S.; Ricci, F.; Vallée-Bélisle, A., *J. Am. Chem. Soc.***2015,** *137*, 15596; c) Du, X.; Jiang, D.; Hao, N.; Qian, J.; Dai, L.; Zhou, L.; Hu, J.; Wang, K., *Anal. Chem.***2016,** *88*, 9622.

(5) a) Huang, X.; Li, L.; Qian, H.; Dong, C.; Ren, J., *Angew. Chem.***2006,** *118*, 5264; b) Yao, H.; Zhang, Y.; Xiao, F.; Xia, Z.; Rao, J., *Angew. Chem. Int. Ed.***2007,** *46*, 4346; c) Xiong, L.; Shuhendler, A. J.; Rao, J., **2012,** 3, 1193; d) Feng, Q.-M.; Shen, Y.-Z.; Li, M.-X.; Zhang, Z.-L.; Zhao, W.; Xu, J.-J.; Chen, H.-Y., *Anal. Chem.***2016,** *88*, 937; e) Algar, W. R.; Khachatrian, A.; Melinger, J. S.; Huston, A. L.; Stewart, M. H.; Susumu, K.; Blanco-Canosa, J. B.; Oh, E.; Dawson, P. E.; Medintz, I. L., *J. Am. Chem. Soc.***2017,** *139*, 363.

(6) a) Suzuki, Y.; Yokoyama, K., *J. Am. Chem. Soc.***2005,** *127*, 17799; b) Ferapontova, E. E.; Olsen, E. M.; Gothelf, K. V., *J. Am. Chem. Soc.***2008,** *130*, 4256; c) Stewart, M. H.; Huston, A. L.; Scott, A. M.; Oh, E.; Algar, W. R.; Deschamps, J. R.; Susumu, K.; Jain, V.; Prasuhn, D. E.; Blanco-Canosa, J.; Dawson, P. E.; Medintz, I. L., *ACS Nano.***2013,** *7*, 9489.

(7) Weimann, A.; Belling, D.; Poulsen, H. E., *Nucleic Acids Res.***2002,** *30*, e7.

(8) Liu, Y.; Wei, M.; Zhang, L.; Zhang, Y.; Wei, W.; Yin, L.; Pu, Y.; Liu, S., *Anal. Chem.***2016,** *88*, 6509.

(9) Zhang, Q.; Wang, Y.; Meng, X.; Dhar, R.; Huang, H., *Anal. Chem.***2013,** *85*, 201.

(10) Kondo, T.; Udagawa, I.; Aikawa, T.; Sakamoto, H.; Shitanda, I.; Hoshi, Y.; Itagaki, M.; Yuasa, M., *Anal. Chem.***2016,** *88*, 1753.

(11) Nelson, D. L.; Cox, M. M., *Lehninger Principles of Biochemistry*. 4th ed.; W. H. Freeman and Company: New York, 2004.

(12) a) Cheng, C.; Huang, Y.; Tian, X.; Zheng, B.; Li, Y.; Yuan, H.; Xiao, D.; Xie, S.; Choi, M. M., *Anal. Chem.***2012,** *84*, 4754; b) Tian, J.; Liu, Q.; Asiri, A. M.; Al-Youbi, A. O.; Sun, X., *Anal. Chem.***2013,** *85*, 5595; c) Rong, M.; Lin, L.; Song, X.; Zhao, T.; Zhong, Y.; Yan, J.; Wang, Y.; Chen, X., *Anal. Chem.***2015,** *87*, 1288.

(13) a) Zhou, Z.; Shen, Y.; Li, Y.; Liu, A.; Liu, S.; Zhang, Y., *ACS Nano.***2015,** *9*, 12480; b) Dong, Y.; Wang, Q.; Wu, H.; Chen, Y.; Lu, C. H.; Chi, Y.; Yang, H. H., *Small.***2016,** *12*, 5376.

(14) Zhang, H.; Li, F.; Dever, B.; Li, X. F.; Le, X. C., *Chem. Rev.***2013,** *113*, 2812.

(15) a) Wang, F.; Lu, C. H.; Willner, I., *Chem. Rev.***2014,** *114*, 2881; b) Zhang, L.; Zhu, J.; Guo, S.; Li, T.; Li, J.; Wang, E., *J. Am. Chem. Soc.***2013,** *135*, 2403.

(16) Park, S.-M.; Yoo, J.-S., *Anal. Chem.***2003,** *75*, 455 A.

(17) Deng, S.; Cheng, L.; Lei, J.; Cheng, Y.; Huang, Y.; Ju, H., *Nanoscale.***2013,** 5, 5435.

(18) Li, T.; Wang, E.; Dong, S., *J. Am. Chem. Soc.***2009,** *131*, 15082.

(19) Liu, S.; Wang, C.; Zhang, C.; Wang, Y.; Tang, B., *Anal. Chem.***2013,** *85*, 2282.

(20) Liu, Z.; Qi, W.; Xu, G., *Chem. Soc. Rev.***2015,** *44*, 3117.

TOC image

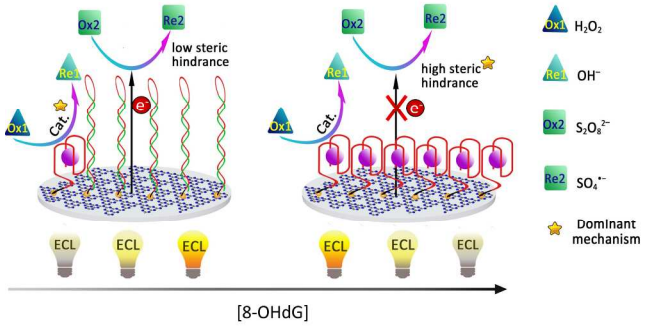
Ox2
Re2
low steric hindrance
Re1
Ox1
Cat.
e⁻
ECL
ECL
ECL
Ox2
Re2
high steric hindrance
Re1
Ox1
Cat.
e⁻
ECL
ECL
ECL
[8-OHdG]
Ox1 H2O2
Re1 OH⁻
Ox2 S2O8 2−
Re2 SO4 •−
Dominant mechanism